Food and Chemical Toxicology 130 (2019) 1–11

Contents lists available at ScienceDirect

Food and Chemical Toxicology

journal homepage: www.elsevier.com/locate/foodchemtox

Final-2 targeted glycolysis mediated apoptosis and autophagy in human lung adenocarcinoma cells but failed to inhibit xenograft in nude mice

Zisheng Chen[a,b], Dacheng Yang[b], Xinwei Jiang[b], Lingmin Tian[b], Jianxia Sun[c], Dongbo Tian[a], Weibin Bai[b,*]

[a] Department of Respiratory Medicine, The Sixth Affiliated Hospital of Guangzhou Medical University, Qingyuan People's Hospital, Qingyuan, China
[b] Department of Food Science and Engineering, College of Science and Technology, Jinan University, Guangzhou, China
[c] Faculty of Chemical Engineering and Light Industry, Guangdong University of Technology, Guangzhou, China

ARTICLE INFO

Keywords:
Non-small cell lung cancer
Cudrania tricuspidata
Kras mutation
Final-2
Autophagy

ABSTRACT

Natural products derived from fruits have multiple antitumor potential. However, very few have been developed for clinical therapy, due to the limited efficiency or insufficient study of their mechanism. Since lung cancer is the most common cancer in the world, there is still need to explore novel compounds but their molecular mechanisms remain elusive. In this study, a new compound Final-2 was synthesized. Final-2 exhibited antitumor activity in A549 cells by promoting apoptosis and blocking autophagy. Moreover, Final-2 significantly induced G_0/G_1 cycle arrest and inhibited cell malignancy. Intracellular molecular targets investigation showed that Final-2 inhibited the Gluts, which resulted in downregulation of glucose metabolism and the oncogene c-Myc and Kras expression in vitro. However, according the autophagy inhibitor CQ and Kras inhibitors test, low concentration of Final-2 showed some controversial effects. In A549 xenograft mice model, 10 mg/kg and 20 mg/kg of Final-2 showed no and partial tumor inhibition, respectively. Moreover, a high dose of Final-2 induced serious liver necrosis. Therefore, the results indicated that even though Final-2 was efficient in suppressing the cancer cell growth in vitro, it failed to inhibit tumors in vivo and showed significant liver toxicity, which was its limitation as a potential antitumor drug.

1. Introduction

Lung cancer includes non-small cell lung cancer (NSCLC) and small cell lung cancer. GLOBOCAN 2018 estimates the lungs to be the first cancer site in most new cases and leads to death for every 36 cancer cases (Bray et al., 2018). As for China, lung cancer is the most commonly diagnosed form of cancer in men and the second most frequently diagnosed in woman, accounting for 23.03% and 16.20% of all new cases respectively (Chen et al., 2015). The crude incidence rate of lung cancer is 46.08 per 100,000, and the mortality rate is about 37.00 per 100,000 (Chen et al., 2015). Recently, scientists have made some breakthrough in new therapeutic strategies including stereotactic ablative RT (SABR), targeted therapies, and immunotherapies. However, only 17.7% of all lung cancer patients survive for more than 5 years after diagnosis (Ettinger Ds Fau – Wood et al., 2017). Despite the rapid advances in treatment for lung cancer, the efficacy of these treatments combined remains limited. Thus, new effective anti-lung cancer drugs are urgently needed. Kras oncogenic mutation is the most commonly detected in NSCLC patients, and it is found in 25%–35% of newly diagnosed NSCLC, especially in lung adenocarcinomas (Kempf et al., 2016). In the current era of precision medicine, selectively treating Kras-mutated NSCLC remains a challenge (Kempf et al., 2016).

In our previous study, three compounds were extracted from *Cudrania tricuspidata* fruit (Li et al., 2018), including: 4-O-Methylalpinumisoflavone, alpinumisoflavone, and scandenolone. It was fund out that scandenolone was the most efficient compound of the three, it directly gotattached to the ATP-binding site for EGFR, downregulated Akt/mTOR/ERK signaling pathway, induced cells apoptosis and blocked autophagy flux in SK-MEL-28 cells (Hu et al., 2017). Analysis of the chemical structure of the three compounds revealed that there was one isopentenyl in scandenolone, which constituted the main anticancer molecular structure because it was not contained in the other two compounds. Therefore, it was hypothesized that adding one more isopentenyl to the scandenolone structure would increase the anticancer activity. Therefore, an isoprenyl was successfully attached to the scandenolone's isoprenyl site and named Final-2, which had a purity of more than 98%. Newly synthetic high purity compounds CY and CCY were used as controls.

* Corresponding author.
E-mail address: baiweibin@163.com (W. Bai).

https://doi.org/10.1016/j.fct.2019.04.054
Received 27 February 2019; Received in revised form 22 April 2019; Accepted 29 April 2019
Available online 01 May 2019
0278-6915/

In the current study, a mechanism underlying the inhibition of glucose metabolism and oncogene c-Myc and Kras by Final-2 was revealed to explain the bioactivity of Final-2 against lung cancer progression. However, it was confirmed through a nude mice model that low dose of Final-2 didn't inhibit A549 xenograft, while relatively high dose of Final-2 partially inhibited the tumor, but a very serious local liver tissue necrosis was noticed. Therefore, final-2 is not an ideal antitumor drug, and more attention should be focused on the potential digestive system toxicity of such food-borne isoflavones.

2. Materials and methods

2.1. Reagents and cell culture

K-Ras(G12C) inhibitor 12 (Kras-I) was purchased from APExBIO (Houston, TX, USA). Rapamycin was obtained from Selleck Chemicals (Houston, TX, USA). Chloroquine (CQ), MTT (3-(4, 5- dimethylthiazol-2-yl)-2, 5-diphenyltetrazolium bromide) and cisplatin were acquired from Sigma (St. Louis, MO, USA). Cell Cycle Analysis Kit and Annexin V-FITC/PI Kit were purchased from 4A Biotech (Beijing, China). ATP Assay Kit was obtained from Beyotime Biotech (Shanghai, China). 2-NBDG was acquired from Cayman Chemical (Ann Arbor, Michigan, USA). L-Lactate Assay Kit I was purchased from Eton Bioscience (San Diego, CA, USA). Antibodies against CDK4, Cyclin D1 and Phospho-Cdc2 (T161) were purchased from Immunoway (Plano, TX, USA). GAPDH, Bax, Glut-1, Glut-4, LDHA, β-tubulin, c-Myc and Phospho-AMPKα were obtained from Cell Signaling Technology (Beverly, MA, USA). P62 and Kras were acquired from Proteintech (Wuhan, China). Glut-3 and MMP-2 were purchased from Santa Cruz Biotech (Dallas, Texas, USA). LC-3 was obtained from Novus Biologicals (Littleton, CO, USA). MMP-9 and Bcl-2 were acquired from Bioss (Beijing, China).

Human lung cancer cells A549 (Derived from ATCC and with a Kras (G12S) mutation), 95-D, H1975, SK-MES-1, H1299 and immortalized human epithelial cells (BEAS-2B) were cultured in DMEM. Immortalized human liver cells (HL7702) were cultured in RPMI-1640 medium (Sigma, St. Louis, MO, USA). All the culture medium was supplemented with 10% fetal bovine serum (FBS, Gibco) in a humidified atmosphere containing 5% CO_2 at 37 °C.

2.2. Cell viability assay, colony formation assay, cell scratch test, and uncoated transwell assay

A549, 95-D, H1975, SK-MES-1, H1299, BEAS-2B and HL7702 were seeded overnight in 96-well plates (1×10^4 cells/well). The cells were then treated with indicated concentrations of Final-2, CY, CCY, and cisplatin. Cell viability was measured using MTT. The absorbance of the samples was measured by a Microplate Reader (Infinite F50, TECAN) at 492 nm.

For colony formation, adherent cells were trypsinized, after which 250 cells/well were seeded in 6-well plates. The cells were allowed to form colonies for 10 days. After removing the medium, the cells were fixed for 15 min with 75% ethanol and stained with crystal violet for visualization.

For cell scratch test, A549 cells were firstly trypsinized and seeded in 6-well plates at 4×10^5 cells per well overnight. A 200 microliter pipette was used to draw across the middle of each well and the suspended cells were removed by washing three times with cold PBS buffer. Subsequently, the cells were treated with indicated concentrations of Final-2 containing 1% fetal bovine serum. The cells were evaluated under the microscope at each indicated time point.

Cell invasion was assessed by Matrigel Transwell (Corning Costar, Corning, NY, USA). A549 cells (1×10^5/mL, 200 μL) were suspended in serum-free medium and seeded in the upper chamber of the Transwell unit, whereas the bottom chamber contained 600 μL medium with 10% FBS. Cells were cultured at 37 °C in a humidified atmosphere with 5% CO_2 for 36 h. The chamber was washed twice with PBS, after which 75% ethanol was added and incubation was carried out for 20 min to fix the invaded cells. After discarding the ethanol, the cells were stained using 0.1% crystal violet, then viewed under an inverted microscope.

2.3. Flow cytometric (FCM) analysis of the cell cycle and apoptosis

A549 cells incubated with different concentrations of Final-2 were harvested after 24 h for cell cycle and apoptosis analysis. For cell cycle analysis, cells were washed twice with cold PBS, then fixed with 75% ethanol for 24 h. After adding 0.4 mL staining buffer, 15 μL PI (25×) and 2 μL RNase (5 mg/mL), the cells were incubated in the dark at 37 °C for 30 min. The cell cycle was analyzed by flow cytometry (BD, Biosciences) at 488 nm. For apoptosis, cells were re-suspended in 100 μL 1 × binding buffer at a concentration of 1–5 × 10^6 cells/mL. 5 μL Annexin V/FITC was added into the cells and incubated in dark at room temperature (RT) for 5 min, 10 μL PI (20 μg/mL) and 400 μL 1 × binding buffer were then added to each tube. Apoptosis was analyzed by flow cytometry at 630 nm and 525 nm.

2.4. L-Lactate Assay

A549 cells were seeded overnight in 96-well plates (1×10^4 cells/well). The cells were then treated with indicated concentrations of Final-2. Based on manufacturer's protocol for L-Lactate Assay Kit I, L-Lactate Standard at a concentration of 3.125 μL, 6.25 μL, 12.5 μL, 25 μL, and 50 μL were added to each well and the volume was adjusted to 50 μL with dH_2O for a Standard Curve. 50 μL L-Lactate Assay solution was added to each well containing the L-Lactate Standards and test samples. The plate was incubated for 30 min at 37 °C and the absorbance was then tested at 492 nm using a microplate reader.

2.5. ATP assay

A549 cells were planted overnight in 12-well plates (8×10^4 cells/well). The cells were then treated with indicated concentrations of Final-2. The medium was then aspiratedand 100 μL ATP lysis buffer was added according to ATP Assay Kit manufacturer's protocol. The mixture was then centrifuged at 12,000 g for 5 min at 4 °C. The supernatant was collected for testing. 0.01 μM, 0.05 μM, 0.25 μM, 1.25 μM, 6.25 μM and 31.25 μM of ATP Standard were added to each well, the volume was then adjusted to 150 μL with ATP lysis buffer to obtain a Standard Curve. 1×ATP test solution was added to each well for 3 min at RT, 50 μL cell supernatant was then added and a Luminescence Microplate Reader (Infinite M200PRO, TECAN) was used to measurethe integration time from 0.25 to 1 s.

2.6. Glucose uptake 2-NBDG, mitochondrial mass Mitotracker green TM

Glucose uptake in A549 cells was quantified using a green fluorescent glucose analog (2-NBDG, Cayman). The cells were incubated in glucose-free DMEM with 10% FBS, containing 100 μg/mL 2-NBDG for time intervals ranging from 0 to 30 min. For Mitotracker green TM (MTG), the cells were incubated in FBS-free RPMI-1640 containing 40 nM MTG for 15 min. 2-NBDG and MTG uptake was analyzed using a flow cytometer. The data was analyzed using FlowJo X software (FlowJo).

2.7. Western blot analysis

Cell lysates were prepared by incubating A549 cells in RIPA buffer (Beyotime, Shanghai, China) with PMSF and phosphatase inhibitor (Beyotime, Shanghai, China) on ice for at least 15 min. After centrifuging at 12,000 g for 12 min, BCA Protein Assay Kit (Beyotime, Shanghai, China) was used to quantify the amount of protein in the supernatant. The samples were boiled with 5×SDS loading buffer at 100 °C for 10 min. Equal amounts of protein were subjected to SDS-

PAGE, after which they were transferred to a PVDF. Membranes were blocked with 5% non-fat milk for 1 h at RT and then incubated with the specific antibodies at 4 °C overnight. The membranes were washed 3 times with TBST and then incubated with specific secondary antibodies for 1 h at RT. Protein signals were visualized using a chemiluminescence system (Clinx, Shanghai, China).

2.8. Animal models

A549 xenograft mice model was established using 6-weeks old male BALB/c nude mice (Guangdong Medical Laboratory Animal Center, GDMLAC). Each mouse was subcutaneously injected with 2×10^6 A549 cells on both sides of the lateral hind legs. When the tumor volume reached 70 mm^3, the mice were randomly assigned to three groups and gastric administered with Final-2 (10 mg/kg), Final-2 (20 mg/kg) or vehicle (0.9% saline with 88% + 10%DMF with 10% + Tween 80 with 2%) every day. All mice were sacrificed after 12 days, and the body weights and tumor volumes (length × $width^2$/2) were determined. Various tissue samples were then collected and fixed with 4% paraformaldehyde for 24 h, after which they were embedded in paraffin. Sections of the heart, liver, spleen, stomach, lung and kidney tissues were stained using hematoxylin and eosin. Animal experiments were carried out in accordance with the Guide for the Care and Use of Laboratory Animals, and the experiments were approved by the animal ethics committee of Jinan University.

3. Results

3.1. Compounds extraction from Cudrania tricuspidata fruit

Scandenolone was firstly isolated from *Cudrania tricuspidata* fruit. For the specific extraction and purification methods refer to our previous study (Hu et al., 2017). To enhance the bioactivity of the compound, isopentenyl was added to the isopentenyl site of the scandenolone, and the end product was named Final-2. To further evaluate the function of isopentenyl in the isoflavone structure, a compound was synthesized without isopentenyl, and named CY. Subsequently, an isopentenyl group was grafted to the CY, and named CCY (Fig. 1).

3.2. Selectively inhibitory effects of Final-2 on human lung cancer cells

Cells viability were evaluated by the MTT assay in human NSCLC cell lines. The effect of Final-2, CCY, CY, and cisplatin was tested in the concentration range of 5–30 μM. Final-2 and CCY significantly reduced cell viability of A549, 95-D, SK-MES-1, and H1975 cells within 24 h in a dose-dependent manner, except in H1299 cells (Fig. 2A). Besides, two normal human cell lines including, lung epithelial cell BEAS-2B and liver cell HL7702 were used to investigate the toxicity of Final-2 and CCY, and to determine the compound to use in the subsequent experiments. Both final-2 and CCY significantly reduced cell viability of BEAS-2B and HL7702, however, CCY showed more serious cytotoxicity on BEAS-2B than in Final-2 (Fig. 2B). Moreover, Final-2 showed a time-dependent suppression of A549 and 95-D cell viability (Fig. 2C). Thus, this study focused on A549 cells line with Kras mutations.

3.3. Final-2 induces cell cycle arrest and inhibits migration in A549 cells

To investigate whether Final-2 affects the cell cycle arrest, A549 cells were stained with PI and then analyzed by flow cytometry. A549 cells were treated with indicated concentrations of Final-2 for 24 h. As shown in Fig. 3A, with the increasing concentrations of Final-2, A549 cell cycle was arrested in G_0/G_1 phase, while the cells proportion in S phase significantly decreased. CDK4 and CyclinD1 are two key regulators of G_0/G_1 phase, Western blot showed that Cyclin D1 and CDK4 expression were reduced. p-Cdc2 (T161) is a marker for G_2/M cycle arrest activation, however, there was no difference after each treatment. Investigations on whether Final-2 affected the malignancy of A549 cells were also carried out and it was found that Final-2 inhibited A549 cells colony formation, invasion, and migration (Fig. 3C, D and 3E). Moreover, treatment with Final-2 resulted in downregulation of the MMP-2 and MMP-9 protein levels (Fig. 3B). This data indicate that Final-2 significantly induced G_0/G_1 cell cycle arrest and result in inhibition of the colony formation, migration, and invasion in A549 cells.

3.4. Final-2 induces A549 cells apoptosis

Changes in the morphology of Final-2-treated A549 cells were observed by an inverted microscope to confirm whether treatment with Final-2 leads to cell death through apoptosis. As seen in Fig. 4A, the number of A549 cells significantly decreased as the concentration of Final-2 was increased. MTT assay also confirmed that Final-2 noticeably inhibited the growth of A549 cells (Fig. 2A). More importantly, treatment with Final-2 resulted in the cells shrinkage, rounding, and detachment. The activation of apoptosis in A549 cells was further analyzed by Annexin V-FITC/PI dual labeling followed by flow cytometry. As the concentration of Final-2 was increased, the proportion of apoptosis in A549 cells increased, and there was a large amount of cell necrosis at 30 μM (Fig. 4B). The expression of anti-apoptotic protein Bcl-2 decreased whereas the expression of pro-apoptotic protein Bax elevated after treatment with Final-2 in a dose-dependent manner (Fig. 4C). Western blotting was performed to measure the expression of Bcl-2 and Bax protein compared to GAPDH (Fig. 4D).

3.5. A549 cellular energy homeostasis is altered by Final-2

The intracellular energy status was also investigated. Firstly, the differences in glucose uptake, intracellular lactate and ATP production with the various doses of Final-2 in A549 cells were determined. As assessed by 2-NBDG, glucose uptake in the A549 cells was significantly decreased after treatment with Final-2 (Fig. 5A). Moreover, low concentration of Final-2 promoted intracellular lactic production, and high concentration of Final-2 downregulated intracellular lactate in A549 cells after 24 h of treatment with Final-2, suggesting that the lactate production was inhibited (Fig. 5B). Intracellular ATP production always decreased after 24 h of treatment with high concentration of Final-2, similarly, low concentration of Final-2 promoted ATP production (Fig. 5C). Furthermore, Mitotracker green TM detected mitochondrial mass and observed that a low concentration of Final-2 caused a slight increase in mitochondrial fluorescence intensity (Fig. 5D). Glucose transporter was further detected by Western blot. The results showed that the expressions of glucose transporters Glut1, Glut2, and Glut3 were significantly inhibited with increasing concentration of Final-2 for 24 h (Fig. 5E).

3.6. Final-2 blocks A549 cells autophagy flux through inhibited AMPK-Gluts in vitro, but a low concentration of Final-2 relieves autophagy inhibition

The process of Warburg Effect in cancer cells means that glucose uptake significantly increases and lactate is produced (Liberti and Locasale, 2016), and oxidative phosphorylation, glycolysis, glutaminolysis, and autophagy are the four sources of ATP in the cells (Oronsky et al., 2014). It was found that low concentrations of Final-2 promoted tumor proliferation (Fig. 2A), it is also well known that autophagy is a kind of orderly degradation and recycling of cellular components (Mizushima and Komatsu, 2011). To confirm the hypothesis in this study, the effect of autophagy inhibitor chloroquine (CQ) on the viability of A549 cells was firstly analyzed, and the results showed that CQ decreased the activity of A549 cells in a concentration-dependent manner (Fig. 6A). However, with increasing concentration of autophagy inducer rapamycin did not show that cell viability decreased in a concentration-dependent manner (Fig. 6B). This indicates that

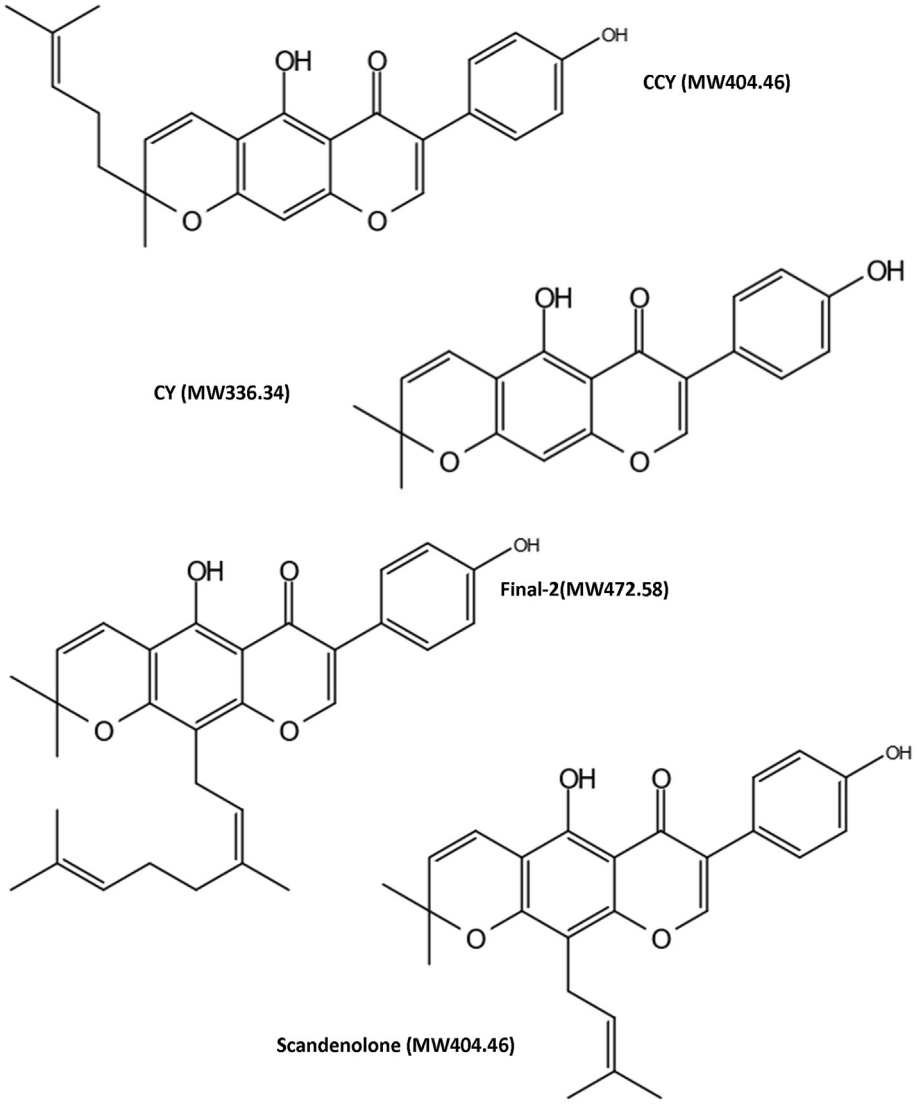

Fig. 1. Chemical structure of scandenolone, Final-2 and other comparative compounds.

inhibition of autophagy causes cell death. Furthermore, the expression of p62 and LC3-II are widely regarded as an autophagosome marker. As shown in Fig. 6C, with the increasing concentration of Final-2, the expression of p-AMPK was downregulated in a concentration-dependent manner, while the accumulation of p62 and LC3-II protein was observed. Meanwhile, the oncogenes c-Myc and Kras were downregulated in a concentration-dependent manner. Previous experiments have shown that Final-2 reduces the expression of Glut1, Glut3 and Glut4 in a concentration-dependent manner (Fig. 5E). These results suggest that Final-2 blocks autophagy flux by downregulation of AMPK-Gluts, oncogenes Kras and c-Myc, and causes A549 cells death.

Investigations were carried out on whether low concentrations of Final-2 promoted survival by relieving inhibition of autophagy. 20 μM Final-2 were added to different concentrations of CQ for co-culture and it was found that Final-2 significantly relieved CQ autophagy inhibition (Fig. 6D). Kras inhibitor (K-Ras (G12C) inhibitor 12) significantly reduced the cell viability of A549, and the presence of a low concentration of Final-2 remarkably increased the survival rate of A549 cells. Moreover, as the concentration of Final-2 increased, its toxicity to normal airway epithelial cells and hepatocytes became more pronounced (Fig. 2B). These results indicate that the anticancer effect of Final-2 in vitro could be only an illusion and may not be effective in vivo.

3.7. Final-2 fails to inhibit A549 xenograft in nude mice

To confirm the hypothesis in this study, animal experiments (Fig. 7A) were conducted. A549 cells xenograft studies indicated that administration 10 mg/kg of Final-2 promoted tumor growth, and a partial tumor suppression effect was exhibited at a dose of 20 mg/kg (Fig. 7B). However, in vitro and in vivo liver damage were aggravated with increasing dose (Figs. 2B and 7E). Moreover, the toxic damage of nude mice was manifested in the increase in wet liver weight with increasing dose of Final-2, while the body weight and spleen wet weight were decreased (Fig. 7D and C). However, Final-2 did not show acute toxic reactions in lung, heart, stomach, spleen and kidney tissues in nude mice (Fig. 7F). Collectively, these results indicate that Final-2 not only inhibited A549 cells xenografts, but also exhibited potent liver damage both in vitro and in vivo.

4. Discussion

This study identified the anti-cancer effects of Final-2 in human lung cancer cells in vitro, based on an isoflavone structural modification of scandenolone. A novel metabolism stress mechanism on how Final-2 leads to A549 cell mortality was also presented by assuming that Final-2 targets Kras to inhibit proliferation while simultaneously promoting

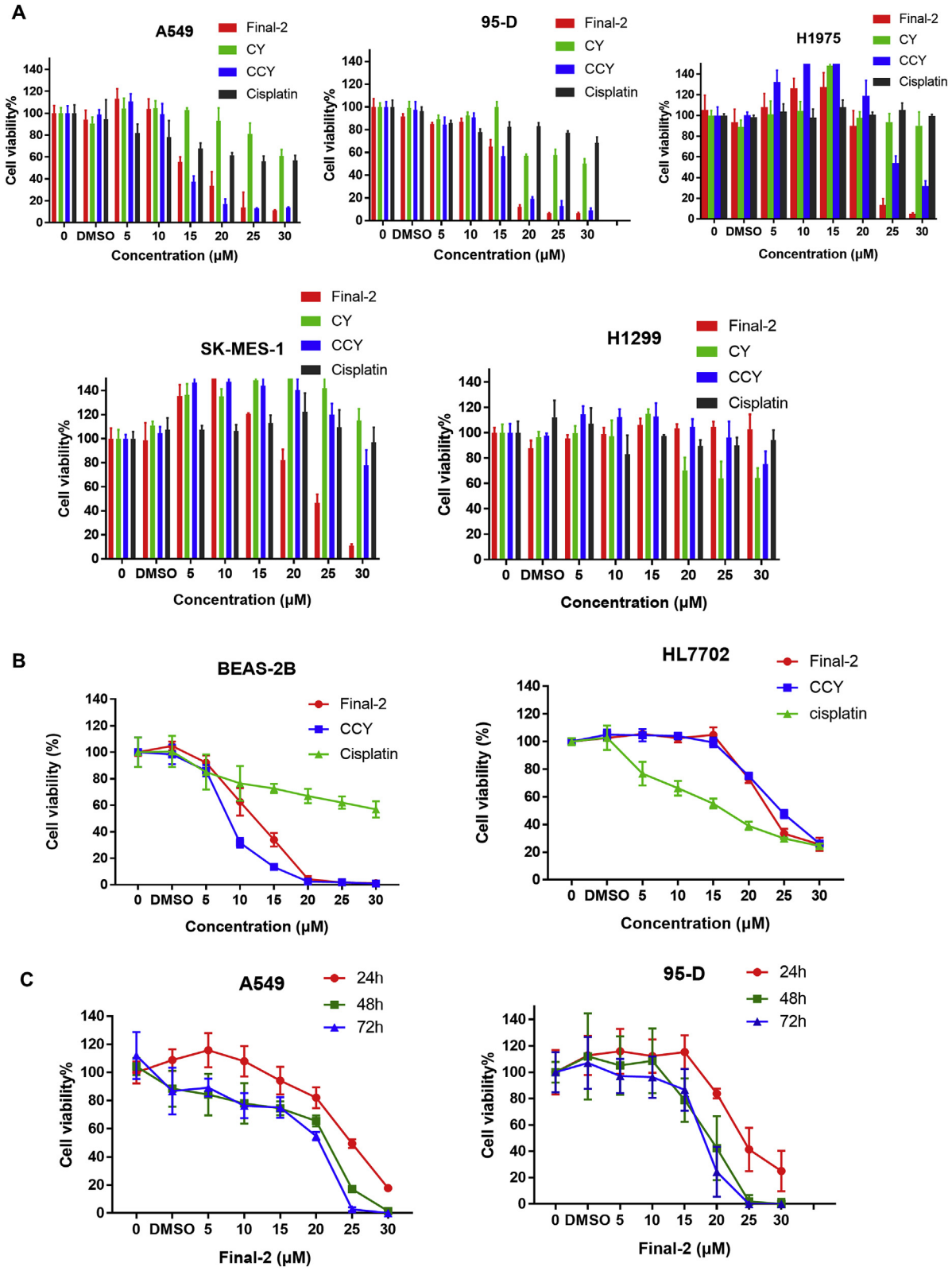

Fig. 2. Final-2 selectively inhibited human lung cancer cell lines. (A) Human NSCLC cells were treated with Final-2, CCY, CY and positive control drug cisplatin at the indicated concentration for 24 h. (B) BEAS-2B and HL7702 cells were treated with Final-2 and CCY at the indicated concentration for 24 h. (C) A549 and 95-D cells were treated with Final-2 at the indicated concentration for 24 h, 48 h, and 72 h. Cell viability was tested using MTT, absorbance was measured by a Microplate Reader at 492 nm.

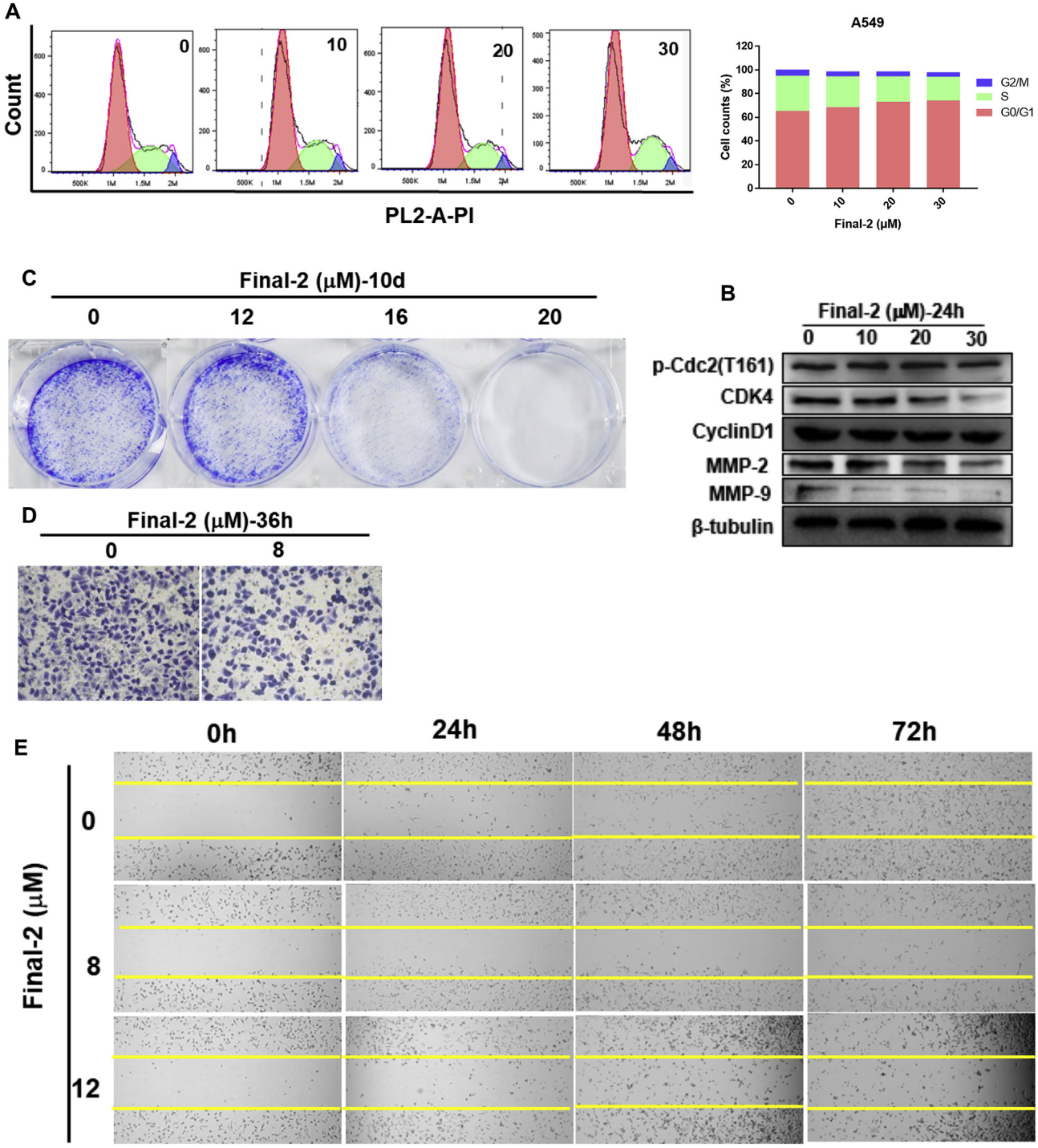

Fig. 3. Final-2 induced the cell cycle arrest and inhibited A549 cell malignancy. (A) Cell cycle distribution as determined by flow cytometry. A549 cells were treated with Final-2 at the indicated concentrations (μM) for 24 h and FlowJo X was used to prepare the percentage histogram of A549 cell cycle. (B) The expression of cell cycle-related proteins and metalloproteins in A549 cells were determined with Western blot after treatment with drugs at the indicated concentrations for 24 h. (C) The inhibitory effect of Final-2 on A549 cell clone formation at the indicated concentrations was observed for 10 days, followed by staining with crystal violet for 15 min and imaging. (D) Images of A549 cells that migrated through the membrane at the indicated concentrations of Final-2 in the uncoated matrigel transwell. (E) Indicated concentrations of Final-2 for 24 h, 48 h and 72 h about cell scratch test, at 12 μM, more cell death began to be seen at 48 h. (For interpretation of the references to colour in this figure legend, the reader is referred to the Web version of this article.)

apoptosis and inhibiting autophagy that would result in cells survival.

As early as 2000, a study reported that the intake of flavonoids rich diets such as onions inversed the risk of lung squamous cell carcinoma (Le Marchand et al., 2000). Christensen KY et al. studies based on a large sample found that the intake of food-borne flavonoid decreased lung squamous cell carcinoma but not the risk of adenocarcinoma's (Christensen et al., 2012). Nowadays, there are about 120 kinds of flavonoids extracted and purified from *Cudrania tricuspidata*, including flavonoids, flavanones, and isoflavones (Xin et al., 2017). The anti-tumor activity of C. tricuspidata in vitro mainly is based on inducing apoptosis (Kwon et al., 2016; Shin et al., 2014) and blocking autophagy flux in cancer cells (Hu et al., 2017). Mouse B16 melanoma and human

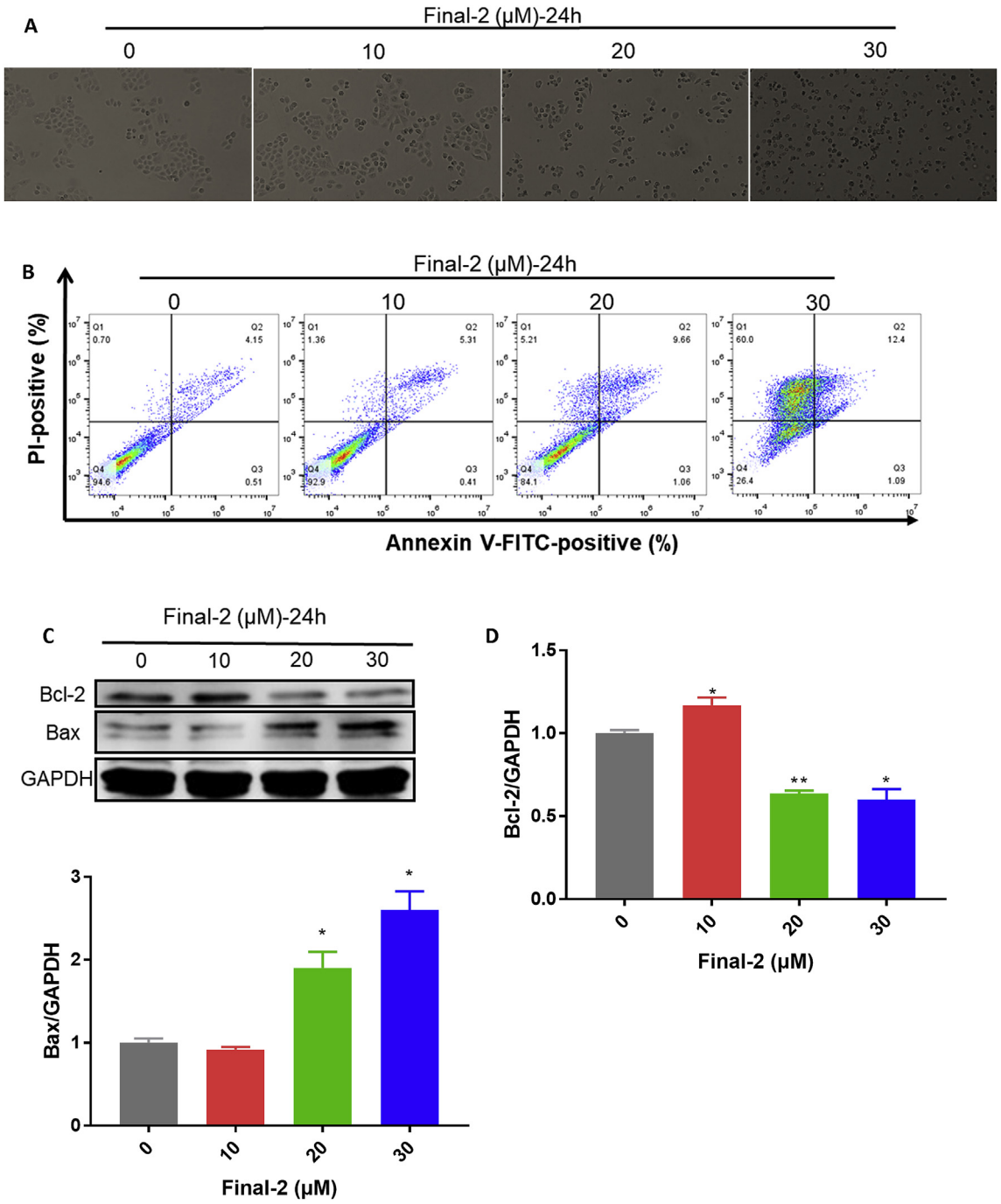

Fig. 4. Final-2 induced apoptotic cell death in A549 cells. (A) Morphology of A549 cells was observed under inverted phase contrast microscope (100×) after treatment with Final-2 at the indicated concentrations. (B) A549 cells were stained with Annexin-V-FITC/PI after treatment with Final-2 at the indicated concentrations. Apoptosis was analyzed by flow cytometry. (C) The protein expressions of Bax and Bcl-2 were detected using Western blot. (D) Effects of Final-2 on Bcl-2 and Bax expressions compared to GAPDH by Western blot analysis. All data are presented as the means ± SD from three independent experiments (n = 3). *P < 0.05 and **P < 0.01 by GraphPad Prism 7.0 Unpaired Student's t-test.

ovarian SK-OV3 xenograft nude mice model results showed that the tumor-inhibiting rates of the total flavonoids derived from C. tricuspidata as large dose of 250 mg/kg were 50.54% and 46.38%, respectively (Xin et al., 2017), but this study did not describe the toxic effects.

C. tricuspidata affects the cancer cell cycle, but different extracts cause different cell cycle arrests depending on the cell type. A previous study showed that scandenolone induced SK-MEL-28 cell cycle arrest at the G_2/M phase (Hu et al., 2017). However, *Cudrania tricuspidata* stem (CTS) extract induced SiHa cervical cancer cells at the G0/G1 phase (Kwon et al., 2016). As expected, CCY and Final-2 with isoprenyl group had better NSCLC cell lines cytotoxicity in vitro, but CCY had greater toxicity to BEAS-2B than to Final-2, thus Final-2 was selected for this study. It was found that Final-2 induced cell cycle arrest at the G_0/G_1 phase by down-regulating CDK4 and Cyclin D1 proteins. However, G_2/M phase activated protein marker p-Cdc2 (T161) expression was not different. Furthermore, the Final-2-mediated downregulation of MMP-2 and MMP-9 inhibited the colony formation, migration, and invasion of A549 cells. These results indicate that Final-2 inhibits the malignancy of A549 cells by inducing cell cycle arrest and down-regulating the activity of matrix metalloproteinases.

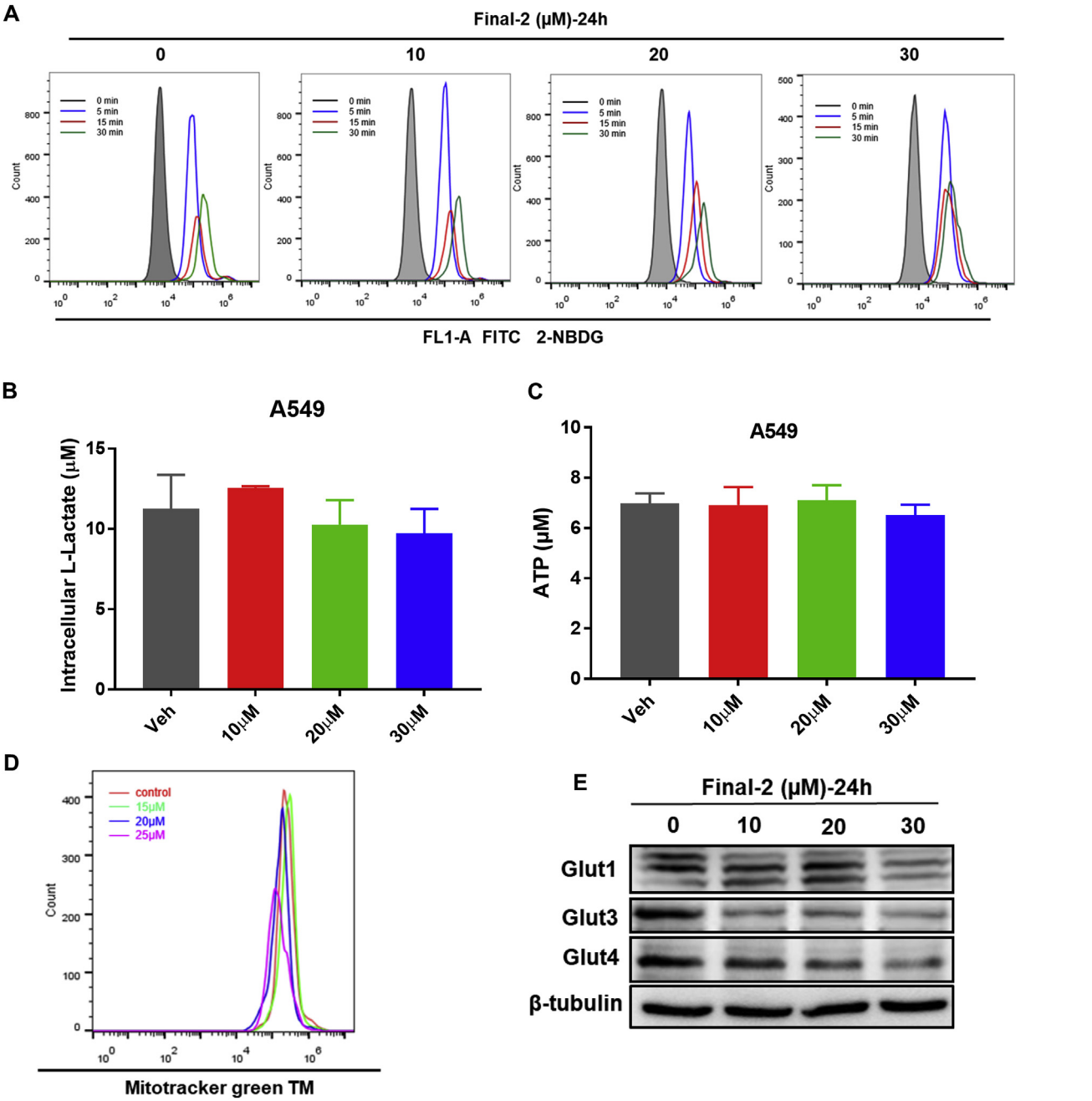

Fig. 5. Final-2 affected intracellular energy homeostasis of A549 cells. (A) A549 cells were treated with Final-2 at the indicated concentrations for 24 h and then incubated with 2-NBDG for the indicated times. 2-NBDG is a green fluorescent glucose analog that is commonly used to determine glucose uptake. 2-NBDG signals were captured using flow cytometry. (B) A549 cells were treated with Final-2 at the indicated concentrations for 24 h, intracellular lactate was measured by L-Lactate Assay Kit I, Final-2 promoted lactic acid production at 10 μM, (C) intracellular ATP was measured by ATP Assay Kit, Final-2 promoted ATP production at 20 μM. (D) A549 cells were treated with Final-2 at the indicated concentrations for 24 h and then incubated with Mitotracker green TM for the indicated time. The cell-permeant Mitotracker green contains a mildly thiol-reactive chloromethyl moiety for labeling mitochondria, Mitotracker green signals were captured using flow cytometry. (E) The protein expression of Glut1, Glut3, and Glut4 were detected using Western blot. (For interpretation of the references to colour in this figure legend, the reader is referred to the Web version of this article.)

The increased Bax/Bcl2 ratio indicated that the mitochondria-mediated apoptosis pathway was activated (Alarifi et al., 2017). This study showed that Final-2 induced apoptosis in A549 in a concentration-dependent manner, and the ratio of Bax/Bcl2 protein significantly increased. The mechanism by which Final-2 induced apoptosis in A549 cells was further explored. Since 2-NBDG is a fluorescent indicator for direct glucose uptake (Zou et al., 2005), the results showed that low concentration of Final-2 did not effectively inhibit glucose uptake, although Western blot results indicated that Final-2 inhibited Gluts such as Glut1, Glut3, and Glut4 in a concentration-dependent manner. Intracellular lactic acid and ATP production did not show significant concentration dependence, but a low concentration promoted the production of lactic acid and ATP. The mitochondrial mass was assessed via MTG, and the results showed that Final-2 didn't decrease mitochondrial mass in a concentration-dependent manner. These results indicate that a relatively high concentration (30 μM) of Final-2 inhibits glucose metabolism and simultaneously induces A549 cells cliff mortality.

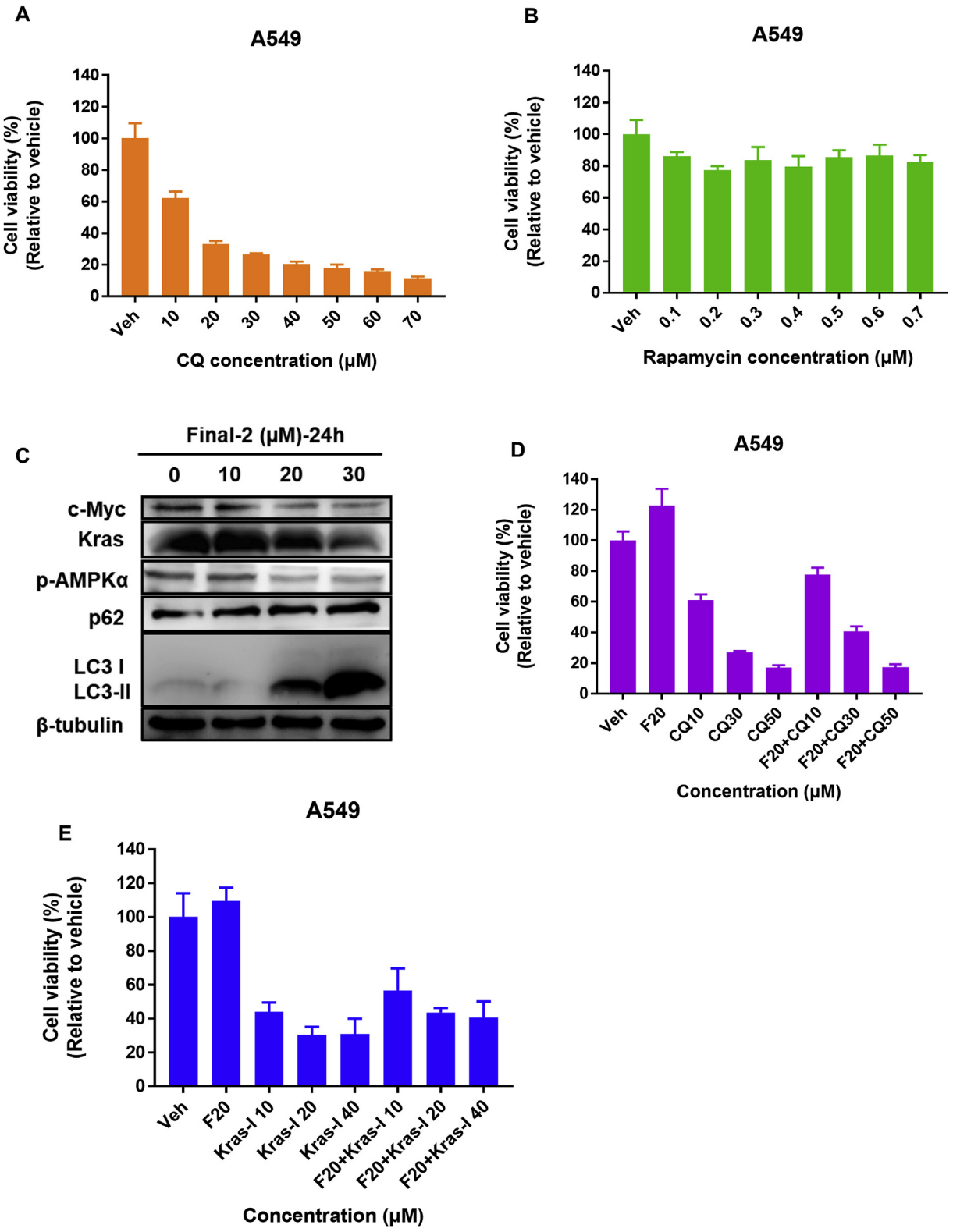

Fig. 6. Final-2 blocks A549 autophagy flux by inhibiting AMPK-Gluts, but a low concentration of Final-2 relieved the inhibition of autophagy and reduced the effect of Kras inhibitors. (A) CQ decreased the cell viability of A549 in a concentration-dependent manner according to MTT test, (B) but this phenomenon was not observed in Rapamycin group. (C) Final-2 inhibited autophagy flux in A549 cells in a concentration-dependent manner, autophagy was measured by p-AMPKα, p62 and LC3-II using Western blot, simultaneously Final-2 inhibited the expression of the oncogenes Kras, c-Myc and Gluts such as Glut1, Glut3, and Glut4 (Fig. 5E). (D, E) Cells were seeded in 96-well plate overnight at a density of 1.5×10^4/well, 20 μM Final-2 (F20) and the indicated concentrations of CQ and K-Ras (G12C) inhibitor 12 (KRas-I) were added to the A549 cells for 24 h. The cell viability was determined by MTT.

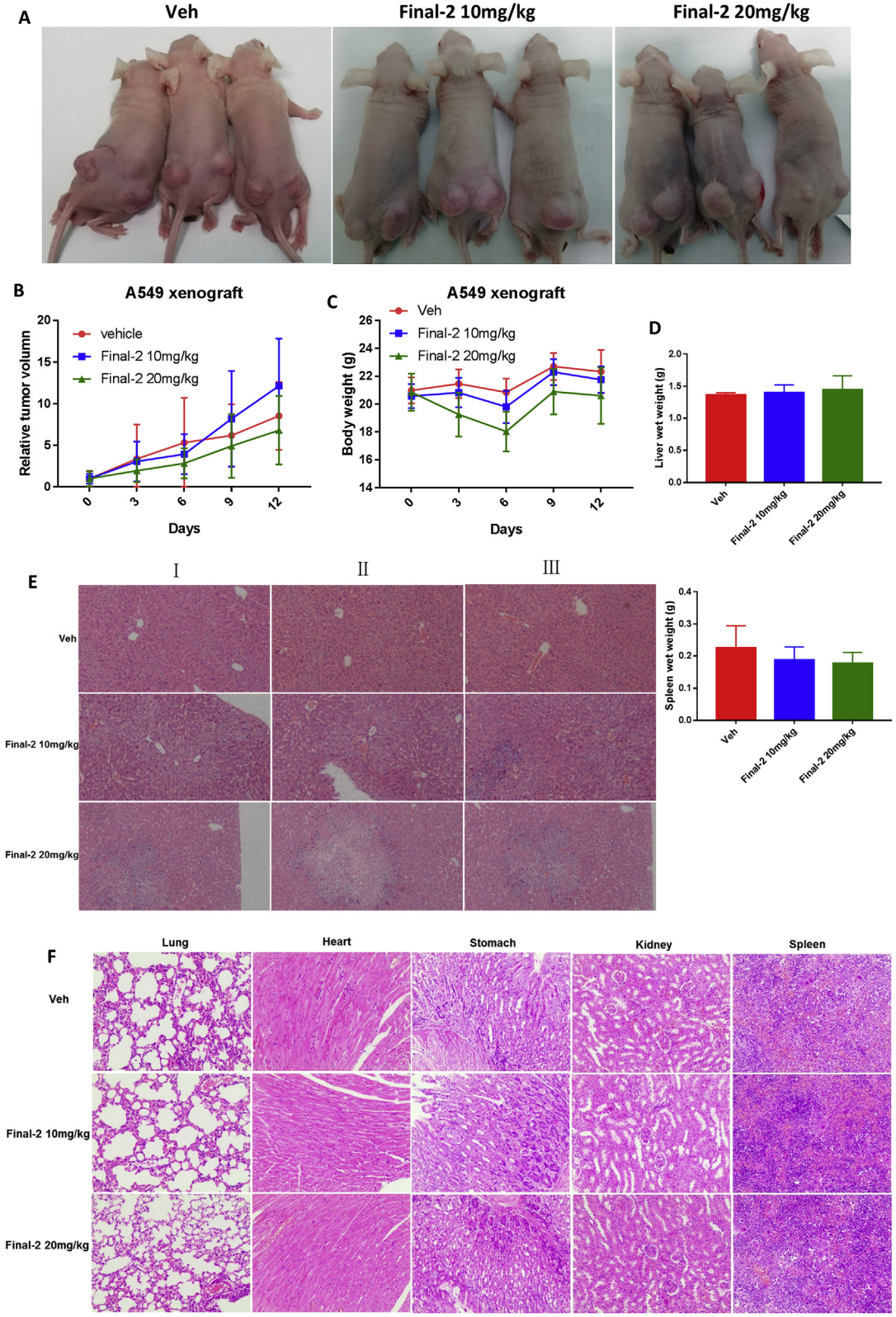

Fig. 7. Final-2 failed to inhibit A549 xenograft in vivo and its potent liver damage both in vitro and in vivo. (A) A549 lung cancer cells 2×10^6/side were injected into the lateral hind limb of male nude mice. When the volume of the xenograft was 70 mm^3, mice were randomly divided into three groups with six mice in each group. Final-2 was administered at the indicated dose for 12 days. Mice were then imaged with a camera. (B) Relative tumor volume and (C) body weight of nude mice treated with vehicle, Final-2 10 mg/kg and 20 mg/kg for the indicated times. (C) Liver wet weight and spleen wet weight after treatment with Final-2 at the indicated dose. (E) After treatment of mice with different doses of Final-2 for 12 days, three liver slices were randomly selected from each group. It was found that the liver structure of the mice in the vehicle group was close to normal. There was widespread inflammatory cell infiltration in the 10 mg/kg Final-2 group and central venous congestion. Local hepatocyte necrosis was found in 20 mg/kg group. (F) Mice were treated with Final-2 at the indicated doses for 12 days, and histopathological analysis of Final-2 in nude mice was detected. The figures shows representative images of the lung, heart, stomach, kidney, and spleen using hematoxylin and eosin.

It was hypothesized that the ability of low concentrations of Final-2 to promote cell proliferation and energy metabolism may be associated with autophagy. Western blot results showed that Final-2 inhibited p-AMPKAα in a concentration-dependent manner, while p62 and LC3-II protein accumulation, simultaneously inhibited oncogenes as c-Myc and Kras. This indicates that Final-2 induces apoptosis in A549 cells by inhibiting autophagy flux in a concentration not leading to the death of most of A549 cell. A relatively low concentration of Final-2 can reduce the autophagy inhibition of CQ, while attenuating the cytotoxicity of Kras inhibitors.

In previous drug research, low concentrations promote the proliferation of cancer cells and cliff-type cell death for relatively high concentration. These type of compounds are mainly composed of Chinese herbal medicine and compounds from plant extract, including C. tricuspidata extracts (Kwon et al., 2016; Lee et al., 2013; Soo et al., 2017; Yao et al., 2017). Many studies have reported that these compounds are effective in inhibiting animal xenograft models (Tsai et al., 2015; Yao et al., 2017). There is a lot of doubt cast on these studies, based on the ability of low concentrations of these compounds to promote proliferation, energy metabolism, while necrosis is reported under their relatively high concentration. In animal xenograft experiments, a low dose may not inhibit tumors, while high dose may have partial inhibitory effects, but toxicity to organs can't be ignored. Based on the Oridonin compound study (Yao et al., 2017), Final-2 was divided into a low-dose of 10 mg/kg and a high dose of 20 mg/kg by administration. The A549 xenograft showed that low-dose did not inhibit the tumor at all, while high-dose partially inhibited the tumor, but the body weight and spleen weight of nude mice significantly decreased and the liver weight was increased. H&E staining of liver tissue under high dose showed more serious local necrosis than under low dose. In the patients of locally advanced NSCLC, spleen volume becomes smaller and its volume could not return to the baseline after 4 weeks of chemotherapy (Wen et al., 2015).

In summary, Final-2 exerts in vitro antitumor activity on A549 cells, and this effect can be explained by the ability of Final-2 to specifically target Gluts activity to impede its glucose metabolism. This interaction is also essential for sensitizing cells to intrinsic apoptosis and blocking autophagy flux and oncogenes c-Myc and Kras. However, Final-2 can't inhibit tumors and it exhibits significant digestive toxicity in vivo. Therefore, it cannot be considered as a potential antitumor drug. More attention should be focused on the potential digestive system toxicity of such food-borne isoflavones.

Declaration of interests

The authors declare that they have no known competing financial interests or personal relationships that could have appeared to influence the work reported in this paper.

Conflict of interest

The authors declare no conflict of interest.

Abbreviations

NSCLC, non-small cell lung cancer; SABR, stereotactic ablative RT; Kras-I, K-Ras(G12C) inhibitor 12; CQ, Chloroquine; MTT, 3-(4, 5- dimethylthiazol-2-yl)-2, 5-diphenyltetrazolium bromide; FCM, Flow cytometric; MTG, Mitotracker green TM; CTS, *Cudrania tricuspidata* stem

Acknowledgments

This study was supported by the Guangdong Key Area Research and Development Program (NO. 2019B020210003). The authors also thank the National Natural Science Foundation of China (NSFC, No. 31871816 and No. 31771978) and the Science and Technology Program of Guangzhou (NO. 201704020050).

Transparency document

Transparency document related to this article can be found online at https://doi.org/10.1016/j.fct.2019.04.054

References

Alarifi, S., Ali, H., Alkahtani, S., Alessia, M.S., 2017. Regulation of apoptosis through bcl-2/bax proteins expression and DNA damage by nano-sized gadolinium oxide. Int. J. Nanomed. 12, 4541–4551.
Bray, F., Ferlay, J., Soerjomataram, I., Siegel, R.L., Torre, L.A., Jemal, A., 2018. Global cancer statistics 2018: GLOBOCAN estimates of incidence and mortality worldwide for 36 cancers in 185 countries. CA A Cancer J. Clin. 68, 394–424.
Chen, Z.M., Peto, R., Iona, A., Guo, Y., Chen, Y.P., Bian, Z., Yang, L., Zhang, W.Y., Lu, F., Chen, J.S., Collins, R., Li, L.M., 2015. Emerging tobacco-related cancer risks in China: a nationwide, prospective study of 0.5 million adults. Cancer 121 (Suppl. 17), 3097–3106.
Christensen, K.Y., Naidu, A., Parent, M.-É., Pintos, J., Abrahamowicz, M., Siemiatycki, J., Koushik, A., 2012. The risk of lung cancer related to dietary intake of flavonoids. Nutr. Canc. 64, 964–974.
Ettinger Ds Fau- Wood, D.E., Wood De Fau- Aisner, et al., 2017. Non-small cell lung cancer, version 5.2017, NCCN clinical practice guidelines in oncology. J. Natl. Compr. Cancer Netw. 15, 504–535.
Hu, Y., Li, Z., Wang, L., Deng, L., Sun, J., Jiang, X., Zhang, Y., Tian, L., Wang, Y., Bai, W., 2017. Scandenolone, a natural isoflavone derivative from Cudrania tricuspidata fruit, targets EGFR to induce apoptosis and block autophagy flux in human melanoma cells. J. Funct. Foods 37, 229–240.
Kempf, E., Rousseau, B., Besse, B., Paz-Ares, L., 2016. KRAS oncogene in lung cancer: focus on molecularly driven clinical trials. Eur. Respir. Rev. 25, 71–76.
Kwon, S.-B., Kim, M.-J., Yang, J.M., Lee, H.-P., Hong, J.T., Jeong, H.-S., Kim, E.S., Yoon, D.-Y., 2016. Cudrania tricuspidata stem extract induces apoptosis via the extrinsic pathway in SiHa cervical cancer cells. PLoS One 11, e0150235.
Le Marchand, L.c., Murphy, S.P., Hankin, J.H., Wilkens, L.R., Kolonel, L.N., 2000. Intake of flavonoids and lung cancer. J. Natl. Cancer Inst. 92, 154–160.
Lee, H.J., Auh, Q.S., Lee, Y.M., Kang, S.K., Chang, S.W., Lee, D.S., Kim, Y.C., Kim, E.C., 2013. Growth inhibition and apoptosis-inducing effects of cudraflavone B in human oral cancer cells via MAPK, NF-kappaB, and SIRT1 signaling pathway. Planta Med. 79, 1298–1306.
Li, X., Yao, Z., Jiang, X., Sun, J., Ran, G., Yang, X., Zhao, Y., Yan, Y., Chen, Z., Tian, L., Bai, W., 2018. Bioactive compounds from Cudrania tricuspidata: a natural anticancer source. Crit. Rev. Food Sci. Nutr. 1–21.
Liberti, M.V., Locasale, J.W., 2016. The Warburg effect: how does it benefit cancer cells? Trends Biochem. Sci. 41, 211–218.
Mizushima, N., Komatsu, M., 2011. Autophagy: renovation of cells and tissues. Cell 147, 728–741.
Oronsky, B.T., Oronsky, N., R Fanger, G., W Parker, C., Z Caroen, S., Lybeck, M., J Scicinski, J., 2014. Follow the ATP: tumor energy production: a perspective. Anti Cancer Agents Med. Chem. 14, 1187–1198.
Shin, M.-R., Lee, H.-J., Kang, S.-K., Auh, Q., Lee, Y.-M., Kim, Y.-C., Kim, E.-C., 2014. Isocudraxanthone K induces growth inhibition and apoptosis in oral cancer cells via hypoxia inducible factor-1α. Biomed. Res. Int., 934691 2014.
Soo, H.C., Chung, F.F., Lim, K.H., Yap, V.A., Bradshaw, T.D., Hii, L.W., Tan, S.H., See, S.J., Tan, Y.F., Leong, C.O., Mai, C.W., 2017. Cudraflavone C induces tumor-specific apoptosis in colorectal cancer cells through inhibition of the phosphoinositide 3-kinase (PI3K)-AKT pathway. PLoS One 12, e0170551.
Tsai, J.-R., Liu, P.-L., Chen, Y.-H., Chou, S.-H., Cheng, Y.-J., Hwang, J.-J., Chong, I.-W., 2015. Curcumin inhibits non-small cell lung cancer cells metastasis through the adiponectin/NF-κb/MMPs signaling pathway. PLoS One 10, e0144462.
Wen, S.W., Everitt, S.J., Bedő, J., Chabrot, M., Ball, D.L., Solomon, B., MacManus, M., Hicks, R.J., Mőller, A., Leimgruber, A., 2015. Spleen volume variation in patients with locally advanced non-small cell lung cancer receiving platinum-based chemo-radiotherapy. PLoS One 10, e0142608.
Xin, L.-T., Yue, S.-J., Fan, Y.-C., Wu, J.-S., Yan, D., Guan, H.-S., Wang, C.-Y., 2017. Cudrania tricuspidata: an updated review on ethnomedicine, phytochemistry and pharmacology. RSC Adv. 7, 31807–31832.
Yao, Z., Xie, F., Li, M., Liang, Z., Xu, W., Yang, J., Liu, C., Li, H., Zhou, H., Qu, L.-H., 2017. Oridonin induces autophagy via inhibition of glucose metabolism in p53-mutated colorectal cancer cells. Cell Death Dis. 8, e2633.
Zou, C., Wang, Y., Shen, Z., 2005. 2-NBDG as a fluorescent indicator for direct glucose uptake measurement. J. Biochem. Biophys. Methods 64, 207–215.